Full Text View

Volume 30, Issue 7 (July 2000)

Journal of Physical Oceanography
Article: pp. 1645–1668 | Abstract | PDF (375K)

Eddy Fluxes and Second-Order Moment Balances for Nonhomogeneous Quasigeostrophic Turbulence in Wind-Driven Zonal Flows*

Dirk Olbers

Alfred Wegener Institute for Polar and Marine Research, Bremerhaven, Germany

Jörg-Olaf Wolff+

Antarctic CRC, Hobart, Australia

Christoph Völker

Institut für Meereskunde an der Universität Kiel, Kiel, Germany

(Manuscript received August 4, 1998, in final form July 27, 1999)
DOI: 10.1175/1520-0485(2000)030<1645:EFASOM>2.0.CO;2

ABSTRACT

The balances of momentum and second-order moments (potential enstrophy, energies, and potential vorticity flux) of wind-driven zonal flow, using a suite of numerical eddy resolving experiments in a two-layer channel, governed by quasigeostrophic dynamics, are investigated. The flow regime in these experiments does not satisfy the usual scaling of quasigeostrophic large-scale dynamics: relative vorticity is a significant contribution to the quasigeostrophic potential vorticity (QPV) in the deep layer and the lateral Reynolds stress divergence is comparable to the interfacial form stress in the top layer. The balances of second-order moments confirm that the eddy-induced fluxes of QPV and layer thickness are downgradient but significant contributions of triple moments occur. Existing parameterizations and scaling laws of the eddy fluxes of QPV and layer thickness are tested against data from the numerical experiments and it is shown that the usual downgradient forms of parameterization with diffusivities chosen from theories of baroclinic instability or homogeneous β-plane turbulence fail in the present flow regime. The authors suggest that the discrepancy is a manifestation of the strong constraint of the fluxes by the balance of momentum in the steady state.

A consistent parameterization for the eddy-induced flux of QPV is derived from the balance of this moment. The flux is produced by a gradient term, whereas the ageostrophic pressure–QPV covariance is the major destruction, with small

but significant contributions from a triple moment divergence. The approximated balance of the QPV flux,

$$\frac{\overline{v'q'}}{\mathcal{T}} = -\overline{v'^2}\frac{\partial \bar{q}}{\partial y} - \frac{\partial}{\partial y}\overline{v'^2 q'},$$

shows that the QPV flux is not completely diffusive (i.e., downgradient the mean potential vorticity) but that there is an additional transport that relates to the eddy flux of the flux of QPV itself. A parameterization of this triple term by the mean relative vorticity is proposed and the resulting new parameterization of the QPV flux is tested in a simple coarse model of the zonal flow.

- Dirk Olbers
- Jörg-Olaf Wolff
- Christoph Völker

1. Introduction

The importance of the mesoscale eddy field for the large-scale circulation of the ocean has been revealed by many observational and theoretical investigations. There is still necessity to parameterize eddy-induced transports of passive and active tracers in the present ocean models. Even in the high-resolution models of basinwide circulations (Böning and Bryan 1996) and World Ocean models (Semtner and Chervin 1992) eddies are only marginally resolved. The oceanographic community is bound to work with these "eddy allowing" models for climate studies of decadal timescales and with even much coarser models (e.g., Bryan and Lewis 1979; Maier-Reimer et al. 1993; England 1993) for long-term climate studies. With aim to improve the performance of such models but also from an intellectual point of view, the oceanographic research is facing the task of devising practical and dynamically consistent closure schemes.

The recent years have seen increased attention attributed to the dynamical role of the eddy fields in the large-scale flow. After a long period of using primitive closures with constant diffusivities, new concepts of parameterization of eddy-induced fluxes have been proposed for the use in coarse ocean models. They are mostly borrowed from the atmospheric counterpart of eddy–mean flow interaction in midlatitudes where eddies are generated by baroclinic instability and feed back on the mean zonal circulation (Green 1970; Stone 1972;see also the review by Held and Hoskins 1985). New structural concepts have evolved (Gent and McWilliams 1990; Gent et al. 1995; McDougall and McIntosh 1996). They are mostly guided by considerations of the transformed Eulerian mean circulation (e.g., Andrews et al. 1987), where the eddy effects are separated into eddy-induced mean advection and mixing properties, rather than by investigations of dynamical processes of eddy generation and eddy–mean flow adjustment. Some tests in coarse (Danabasoglu et al. 1994) and high-resolution general circulation models (Rix and Willebrand 1996; Bryan et al. 1999) exist, but a systematic comparison of coarse models with the new implemented closure schemes and truly eddy resolving numerical models has yet to come. A noteworthy exception is the work of Visbeck et al. (1997) where the structural setting of the transformed Eulerian mean circulation, as proposed by Gent and McWilliams, is combined with the parameterizations of eddy transports of heat and salt due to baroclinically unstable eddies, as proposed by Green and Stone. Other practical schemes have been proposed by Treguier et al. (1997) and Killworth (1997).

We pursue a different route of research: we focus on a simpler class of wind and eddy driven circulations—quasigeostrophic flow in a two-layer zonal channel—and derive and test closure schemes by analysis of the relations between the eddy-induced transports and the mean circulation in the "data" from eddy resolving numerical simulations. Quasigeostrophic flow has been extensively studied in atmospheric and oceanographic conditions, both for the investigation of the dynamical balance of zonal flows (e.g., McWilliams et al. 1978; Wolff et al. 1991; Marshall et al. 1993) as well as for the investigation of closure schemes (e.g., Marshall 1981; Ivchenko 1984, 1985a; Vallis 1988; Larichev and Held 1995; Pavan and Held 1996; Held and Larichev 1996). The atmospheric applications are mainly realized in a regime of homogeneous β-plane turbulence where lateral gradients of eddy-induced fluxes do not exist, and the mean flow is uniform. But also the specific forcing implemented in these models—the flow is driven by relaxation to a prescribed homogeneous baroclinic shear flow—prevents a direct transfer of the results to oceanic conditions. Here the flow is forced by a prescribed stress in the surface layer, a narrow eddy-intensified jet develops in both layers and the shear is established by internal flow dynamics.

We study the balances of mean momentum, eddy potential enstrophy, energies and quasigeostrophic potential vorticity (QPV) flux for a suite of 12 numerical experiments, which differ by the parameters of the dynamical system: stratification, differential rotation rate, and parameterization of bottom friction. After exploring the importance and role of the Reynolds and interfacial stresses in the dynamical balance of the mean flow and finding a countergradient behavior of the flux of QPV and layer thickness, we investigate the performance of a diffusive form of these fluxes. In contrast to the homogeneous turbulence regime, where the use of diffusive parameterizations of the eddy-induced QPV transport works successfully (e.g., Pavan and Held 1996), the wind-driven regime defies such a simple approach. We show that experimentally determined diffusivities of the mean QPV and layer thickness cannot be approximated by any of the recently proposed analytical forms derived for infinitesimal perturbations arising from baroclinic instability along the routes of Green (1970)

and Stone (1972), nor by relations resulting from scaling theories for adjusted homogeneous turbulence, as proposed by Larichev and Held (1995) or Held and Larichev (1996).

We attribute the failure to the constraint by the balance of mean momentum. Finally, we investigate the usefulness of these balances—in particular the balance of the QPV flux itself—in deriving a parameterization of the QPV flux. A parameterization of the eddy-induced transport (triple moment) can be given, and a local relation between the QPV flux and the gradient of mean potential vorticity is derived that is not entirely diffusive but includes a nongradient correction due to the triple moment. The new parameterization is tested in a simple coarse model and the momentum dynamics of the zonal flow is analyzed.

2. Quasigeostrophic channel flow

Eddy resolving quasigeostrophic (QG) models in channel geometry are, by now, a standard tool for studying eddy–mean flow interaction in zonal jets (McWilliams et al. 1978; McWilliams and Chow 1981; Wolff and Olbers 1989; Wolff et al. 1991). The model used for this study is described in detail in the latter reference. We give a brief review of the model and discuss the flow regime and dynamics of the experiments.

a. The numerical model

The model describes the flow in a two-layer channel of length Y = 4000 km and width X = 1500 km on a β plane, and the layers have depths H_1 = 1000 m and H_2 = 4000 m. The balance of potential vorticity (QPV)[1],

$$\frac{\partial q_i}{\partial t} + J(\psi_i, q_i) = F_i, \qquad (1)$$

$$q_i = \nabla^2\psi_i \pm \frac{f_0}{H_i}\eta + f, \qquad (2)$$

includes friction terms $F_i = \mathbf{k} \cdot \nabla \times \boldsymbol{\tau}_i/H_i - A_h\nabla^6\psi_i$ where $\boldsymbol{\tau}_1$ is the wind stress vector, and $\boldsymbol{\tau}_2$ is the bottom stress. Subgrid-scale (SGS) effects are modeled by biharmonic lateral friction with hyperviscosity $A_h = 10^{10}$ m^4 s^{-1}. It reflects the parameterization of subgrid momentum transport and serves as energy and enstrophy dissipation. The elevation of the interface is expressed in terms of the geostrophic streamfunction by $\eta = (f_0/g^*)(\psi_2 - \psi_1)$, with $f_0 = -1.263 \times 10^{-4}$ s^{-1} and reduced gravity g^*. Lateral boundary conditions $\nabla^2\psi_i = 0$, $\nabla^4\psi_i = 0$ on both walls (the latter establishes zero momentum flux) and integral auxiliary conditions (McWilliams 1977) are standard. A fourth-order accurate formulation of the Jacobian (Arakawa 1966) turned out to be necessary to compute the second-order eddy balances correctly (Wolff et al. 1993). The wind stress is zonal and zonally constant,

$$\tau_1 = \tau_0 \sin\frac{\pi(y + Y/2)}{Y} \qquad (3)$$

with amplitude $\tau_0 = 10^{-4}$ m^2 s^{-2}. The frictional stress at the bottom is taken either as a linear or quadratic functional of the bottom velocity, that is,

$$\boldsymbol{\tau}_2 = -\epsilon H_2\mathbf{u}_2 \quad \text{or} \quad \boldsymbol{\tau}_2 = -\mu H_2|\mathbf{u}_2|\mathbf{u}_2, \qquad (4)$$

where ϵ and μ are the corresponding coefficients of linear or nonlinear bottom friction.

We have performed four suites of numerical experiments to explore the sensitivities of the model to the basic parameters ϵ and μ of friction, differential rotation β, and stratification g^*. The experiments (see Table 1) are named by three letters; those starting with E and D have linear bottom friction, those starting with N and H have nonlinear bottom friction. The E cases have $\epsilon = 10^{-7}$ s^{-1}; for the D cases this value is doubled. The N cases have $\mu = 10^{-6}$ m^{-1}; for the H cases this value is halved. In each suite we have a standard case (*FB, $\beta = 1.1465 \times 10^{-11}$ m^{-1} s^{-1}, $g^* = 0.02$ m s^{-2}) and for each such case there is an offspring with stronger stratification (*G4, doubled g^*) and one with half the β value (*B5). Although the Rossby radius $\lambda = [g^*H_1H_2/(H_1 + H_2)]^{1/2}/f_0$ exceeds the resolution $\Delta x = \Delta y$ = 20 km only by a factor of about 2, the model is eddy

resolving (we have made experiments with higher resolution). We will use the notation $\lambda_i = [g^*H_i]^{1/2}/f_0$ for the Rossby radius scales of the individual layers.

The integration time of all experiments was 110 years, including a spinup of approximately 20 years. The last 90 years of data were used to determine mean values and eddy covariances. For all these experiments we have evaluated the balance of mean momentum and potential vorticity, and a package of second-, third-, and fourth-order moments of turbulence. Table 1 summarizes the transports and energies of the experiments.

b. The flow regime

Figure 1 shows instantaneous and eddy streamfunction fields of our standard experiment EFB at the end of the integration. A narrow jet has developed with a scale, which is much smaller than the channelwide scale of the wind forcing but much larger than the Rossby radius. It meanders significantly with stronger excursions appearing in the upper layer. The eddy field is defined here as deviation from the time and zonal mean circulation. The instantaneous eddy streamfunction fields show an irregular chain of vortices to the north and to the south of the jet center (particularly in the lower layer). The eddies have a tendency toward an ellipsoidal form, leaning into the direction of the jet. This pattern causes the Reynolds stress convergence (see next section) and thus the concentration of the jet (Holland and Haidvogel 1980). The eddy field is highly correlated in the vertical (see section 3d) but not barotropic, the eddies travel eastward relative to the mean flow, as found by McWilliams et al. (1978) for the most unstable mode of similar channel jets.

Figure 2 shows the profiles of the time and zonally averaged zonal velocities of EFB, DFB, NFB, and HFB. The jet is flanked by side lobes having a similar width as the jet. It is unstable in all cases, the mean shear $U = \bar{u}_1 - \bar{u}_2$ is above the critical value of the Phillip's inviscid linear instability criterion, $U > \beta\lambda^2_2$ (it is not exactly applicable here because the current profiles are not meridionally uniform as in Phillips' model). Boundary layers are clearly identified at the walls, the scale of these layers has the size of the internal Rossby radius.

The gradients of mean potential vorticity (Fig. 3 for EFB) reveal the well-known property of the differing signs in the upper and lower layer in all cases, thus the necessary condition of baroclinic instability is satisfied. The necessary condition for barotropic instability is not satisfied: there is no sign change of the barotropic QPV gradient (lower-left panel). We have separated the QPV gradients into the contributions due to the relative, stretching and planetary vorticity showing that stretching is the dominant contribution. This agrees with the generally assumed scaling $(\lambda/L)^2 \ll 1$ of relative to stretching vorticity for a large-scale flow with length scale L. In the lower layer, however, the signs of the relative and the stretching parts differ. In the center of the jet their sizes are merely a factor of three different so they add in a way to make the gradient of the total QPV of the same size but different sign as the gradient of relative vorticity. Relative vorticity may thus not be neglected.

c. The balance of zonal momentum

For QG dynamics the zonally and time averaged equations for the balances of zonal momentum and mass can be written as a balance between the eddy QPV flux and the frictional stresses,

$$\left\{\frac{\partial}{\partial t}\left(H_i\bar{u}_i \mp f_0\int_{-Y/2}^{y}\bar{\eta}\,dy'\right)\right\} = H_i\overline{v_i'q_i'} + \bar{\tau}_i. \qquad (5)$$

The overbar denotes time and zonal mean, $\bar{\tau}_1$ is the zonal wind stress, and $\bar{\tau}_2$ is the zonal bottom stress. SGS friction is omitted because it is negligible in the balance of the mean flow. The time rate of change term is included here for clarity, it is set in curly brackets to indicate that it vanishes due to time averaging. The QPV flux,

$$\overline{v_i'q_i'} = \overline{v_i'\nabla^2\psi_i'} \pm \frac{f_0}{H_i}\overline{v_i'\eta'} = -\frac{\partial}{\partial y}\overline{u_i'v_i'} \pm \frac{f_0}{H_i}\overline{v_i'\eta'}, \qquad (6)$$

is the two-dimensional divergence of the QG form of the Eliassen–Palm flux. It consists of the Reynolds stress divergence and the vertical divergence of the interfacial form stress, the latter is responsible for the vertical exchange of momentum between the layers. The vertical integral of the QPV flux equals the divergence of the vertically integrated Reynolds stress,

$$\frac{\partial}{\partial y}(H_1\overline{u_1'v_1'q_1'} + H_2\overline{u_2'v_2'q_2'}), \quad (7)$$

and integrating further over the channel width, we find the constraint (Bretherton 1966),

$$\int_{-Y/2}^{Y/2} (H_1\overline{v_1'q_1'} + H_2\overline{v_2'q_2'})\, dy = 0, \quad (8)$$

which is central to the conservation of total zonal momentum as a balance between wind stress and bottom stress,

$$\int_{-Y/2}^{Y/2} \left(\left\{ \frac{\partial}{\partial t}(H_1\overline{u}_1 + H_2\overline{u}_2) \right\} - (\overline{\tau}_1 + \overline{\tau}_2) \right) dy = 0. \quad (9)$$

The second-order eddy-induced covariances appearing in the mean balance of momentum (and QPV) are summarized for all experiments in Fig. 4 (see also Fig. 5). The Reynolds stress in the upper layer is characterized by a central convergence of eastward momentum—establishing a countergradient transport of momentum—and divergence on the flanks. The deep stress divergence is considerably smaller (about a factor of 20) and generally also shows a convergence of eastward momentum in the center (a notable exception is the bottom layer Reynolds stress in the E cases). Though there are clear variations in the overall size, the shape of the stress divergences is surprisingly similar (there is almost no change of the zeroes). The overall balance of the system requires that the magnitude of the interfacial stress must correspond to the wind stress. The Reynolds stress is, however, in some sense a free mode of the system. While the system chooses a small Reynolds stress divergence in the deep layer, the significance of Reynolds stress effects in the directly forced top layer contradicts the scaling derived from linear baroclinic instability theory where the ratio of the Reynolds stress and the interfacial stress is to be of order $O(\lambda/L)$. It is the failure of this scaling that discriminates our regime from the conditions investigated in most recent parameterization schemes of broad scale ocean circulation (e.g., Treguier et al. 1997) and homogeneous β-plane turbulence (e.g., Held and Larichev 1996) where Reynolds stresses are neglected or vanish identically, respectively. Due to the balance of the QPV flux and the applied stresses at the top and the bottom the QPV flux has different signs in the layers, which are just contrary to the signs of the mean gradient of QPV. The QPV flux in thus down the gradient of mean QPV.

3. Second-order balances

A traditional way of investigating turbulence closure schemes lies in the analysis of the balance of higher-order moments, notably eddy energies, eddy potential enstrophy, and second-order eddy fluxes. Provided that parameterizations of the triple moments and dissipation terms, appearing in these balances, are available a closed set of equations for the second-order moments can possibly be derived and the eddy fluxes be determined in terms of quantities resolved in a coarse model. This strategy is followed by the research attributed to the parameterization of the vertical heat transport in the atmospheric boundary layer (see, e.g., Lykossov 1995) and the ocean mixed layer (see, e.g., Large et al. 1994). In this section we analyze the balances of eddy potential enstrophy, eddy energies and the eddy induced flux of QPV and layer thickness and, in the next section, investigate their use for finding parameterizations of the eddy-induced fluxes.

Some important second-order scalar fields and fluxes are displayed in Fig. 5 for EFB. The velocity variances are concentrated in the jet and show a strong anisotropy there: meridional velocity fluctuations are almost twice as large as the zonal ones. Outside the jet we find a more isotropic regime. There is a remarkable difference of an order of magnitude in the level of the velocity variances in the two layers. This is even more drastic in the QPV variance where we have a factor of about 100 between the layers. This mismatch carries over to the zonal fluxes of thickness and QPV, which are much larger in the top layer. The zonal QPV fluxes, however, do not reflect the much weaker eddy regime in the bottom layer. They are of similar size, as constrained by the balance of momentum.

a. Eddy potential enstrophy

The time and zonally averaged balance of eddy potential enstrophy (EPE), defined as $\overline{q_i'^2}/2$, is written in the form

$$\left\{ \frac{\partial}{\partial t} \frac{H_i}{2} \overline{q_i'^2} \right\} = -H_i \frac{\partial}{\partial y} \overline{v_i' \frac{1}{2} q_i'^2} - H_i \overline{v_i' q_i'} \frac{\partial \overline{q}_i}{\partial y} + H_i \overline{q_i' F_i'}. \quad (10)$$

The first term on the rhs—the divergence of a triple moment—represents the eddy-induced flux of EPE. The next term is the production or destruction due to the gradient of mean QPV, it describes the exchange with the enstrophy of the mean flow. The last term arises from the friction terms in the QPV balance. In the upper layer it is entirely caused by the parameterized SGS motion, in the lower layer there is also a contribution from the bottom friction of the resolved eddy flow. As shown in the lower-left panel of Fig. 6, the SGS contribution exceeds the resolved part. In some cases, the latter is partly positive but then it is always compensated by the negative SGS part. We refer to $\overline{q_i' F_i'}$ as "EPE sink": it includes, besides the true dissipation of EPE by the enstrophy cascade to small scales, also a divergence of a frictionally induced flux of EPE as well as a vertical flux exchanging EPE between the layers. Due to the sixth-order derivatives of the streamfunction occurring in the biharmonic friction the computational burden, which is necessary to separate the above terms in the numerical code, is very high so we have not performed this step.

Figure 6 shows the zonally averaged EPE balance for EFB. The balances for the upper and the lower layers are similar in structure. The mean gradient term is positive everywhere, that is, the potential vorticity flux is opposite to the gradient (downgradient) of the mean potential vorticity, as found already by inspection of the individual quantities. It is clear that the production and the sink terms must equate in the integrated balance, the triple term is, however, free from such a constraint of balance. The triple term turns out to be of the same magnitude as the production and sink in the middle of the channel (it even exceeds the sink in some cases) and also gives substantial input to the balance in the jet flanks. This disagrees with Shutts (1983), Treguier et al. (1997), and others who have suggested that the triple moment is negligible in large-scale flow. McWilliams and Chow (1981) overestimated the triple moment due to the failure of the Arakawa Jacobian in the enstrophy balance of their model (see Wolff et al. 1993).

The terms in the bottom layer balance are an order of magnitude smaller than those in the top layer but even in this weak eddy regime the eddy-induced transport is significant. We conclude that, at least for the top layer, there cannot be any significant contribution from the above mentioned frictionally induced exchange term in the above separation of $\overline{q_i' F_i'}$. Another outstanding feature of the balance is the local minimum of the sink term in the jet center, which is especially well-pronounced in the lower layer. It mainly arises from the resolved frictional part of $\overline{q_2' F_2'}$ but slight contributions are made by the SGS part as well (see Fig. 6, left lower panel). Because these undulations in the sink terms are in phase in the two layers they cannot represent an exchange between layers, and we must attribute them to a frictionally induced transport divergence, which is part of the sink term. This transport counteracts the transport by the triple moment.

b. Eddy energies

The balances of EPE and eddy available potential energy (EAPE), defined as $g^* \overline{\eta'^2}/2$, are very similar in structure:

$$\left\{\frac{\partial}{\partial t}\frac{g^*}{2}\overline{\eta'^2}\right\} = -g^*\frac{\partial}{\partial y}\overline{v_2'\frac{1}{2}\eta'^2} - g^*\overline{v_2'\eta'}\frac{\partial\overline{\eta}}{\partial y} + \overline{w'(p_2' - p_1')}. \qquad (11)$$

Here p_i is the geostrophic pressure and w the vertical velocity of the interface, which is determined by the divergence of the ageostrophic flow in the bottom layer,

$$w = \frac{\partial\eta}{\partial t} + \mathbf{u}_2 \cdot \boldsymbol{\nabla}\eta = -H_2\boldsymbol{\nabla}\cdot\mathbf{u}_2^{ag}. \qquad (12)$$

As in (10) we notice in (11) the divergence of a triple moment and a production or destruction due to the gradient of mean interface height (it describes the exchange with the potential energy of the mean flow). There is, however, no friction or dissipation term; instead we find a covariance between the vertical velocity and the thickness perturbation, describing the exchange of EAPE and eddy kinetic energy by eddy induced lifting of the interface.

The eddy kinetic energy (EKE) is balanced according to

$$- H_i \overline{u_i' v_i'} \frac{\partial \overline{u}_i}{\partial y} \pm \overline{w' p_i'} + H_i \overline{\mathbf{u}_i' \cdot \mathbf{X}_i'}, \qquad (13)$$

where $\mathbf{X}_i = (X_i, Y_i)$ are the frictional (resolved bottom friction and SGS) terms in the ageostrophic momentum equations. They correspond to the QPV friction term $F_i = \mathbf{k} \cdot \nabla \times \mathbf{X}_i$, as specified in section 2. The ageostrophic fluxes appearing in (13) and the exchange terms between kinetic and potential energy cannot be evaluated from ordinary quasigeostrophic dynamics.[2]

The balances (11) and (13) are displayed in Fig. 7 with the ageostrophic and SGS terms combined as residual imbalance. Consistent with the dynamics of a baroclinically unstable state the eddy system is driven by the transfer to EAPE from the mean baroclinic energy [by the gradient term in (11)] and further transfer to the EKE [by the ageostrophic exchange term in (11)]. The counterpart of the latter transfer is contained in the ageostrophic imbalance in the balance of EKE in Fig. 7. The mean gradient term in the EKE balance is a loss of EKE everywhere in both layers: the energy cycle is closed—apart from the loss due to friction—by the transfer from eddy to mean kinetic energy [by the gradient term in (13)]. Notice that this property implies an upgradient transport of momentum everywhere in the channel. The eddy-induced transport by the geostrophic terms leads to a loss of eddy energy in all three compartments in the jet center and affects a transfer to the jet flanks.

If (11) and (13) are combined to the balance of total vertically integrated energy of the system, the exchange terms between potential and kinetic energy cancel and ageostrophic terms remain only in form of divergences. The balance is displayed in the lower-right panel of Fig. 7. It is seen that the sum of all gradient terms drives the eddy system and bottom friction acts as major sink. There is a small net sink from SGS contained in the imbalance, in EFB it is about 40% of the size of the bottom friction term. The dominant role of the imbalance term is, however, a redistribution by ageostrophic eddy motion which counteracts the geostrophic eddy induced transport.

c. QPV and thickness flux

Finally we consider the balances of the eddy induced QPV flux and thickness flux, which read

$$\left\{\frac{\partial}{\partial t} \overline{v_i' q_i'}\right\} = -\frac{\partial}{\partial y} \overline{v_i'^2 q_i'} - \overline{v_i'^2} \frac{\partial \overline{q}_i}{\partial y} - \beta y \overline{u_i' q_i'} + \mathcal{V}_i + \overline{v_i' F_i'} + \overline{q_i' Y_i'} \qquad (14)$$

$$\left\{\frac{\partial}{\partial t} \overline{v_2' \eta'}\right\} = -\frac{\partial}{\partial y} \overline{v_2'^2 \eta'} - \overline{v_2'^2} \frac{\partial \overline{\eta}}{\partial y} - \beta y \overline{u_2' \eta'} + \mathcal{Q} + \overline{\eta' Y_2'}. \qquad (15)$$

We have combined in the expression

$$\mathcal{V}_i = -f_0 \overline{u_i'^{ag} q_i'} - \overline{q_i' \frac{\partial p_i'^{ag}}{\partial y}}$$

$$\mathcal{Q} = -f_0 \overline{u_2'^{ag} \eta'} - \overline{\eta' \frac{\partial p_2'^{ag}}{\partial y}} + \overline{v_2' w'} \qquad (16)$$

the ageostrophic covariances. We can identify in (14) the divergence of eddy-induced fluxes (by a triple moment) and the production/destruction term associated with the gradient of mean QPV or interface height, respectively. The latter terms describe the exchange of flux with the corresponding transport of mean quantity by the mean current. The meridional flux is coupled by a Coriolis term to the zonal flux. Sink terms are certainly contained in the frictional terms. Contributions in the F' and Y' terms from the (resolved) bottom friction can easily be extracted and evaluated. They are of order ϵ times the flux

and found to be very small. The remaining SGS contributions have not been evaluated separately but are expected to be small as well. The role and magnitude of the ageostrophic terms are not a priori evident.

The QPV flux balance is displayed in the upper panels of Fig. 8 (in contrast to the scalar balances we have not integrated the flux balances over the layer depths). The contribution from the eddy triple flux, the gradient term, and the Coriolis term are shown individually and the ageostrophic terms are again combined in the remaining imbalance. The balance is easily described: the gradient term acts as a source of northward flux and the ageostrophic terms act as a sink. In the upper layer there is a significant contribution from the triple divergence working as destruction in the jet center. The Coriolis term is a small sink, mainly acting in the flank region. It is obvious from (14) that the magnitudes of the balance terms in the two layers are roughly in proportion to the velocity variance. The balance of thickness flux, shown in the lower panel of Fig. 8, closely corresponds to the balance pattern of the QPV flux. Coriolis and triple terms are here negligible.

d. Timescales of second-order balances

Though we have a drastic difference in the overall size of the balance rates of EPE in the two layers (see Fig. 6), this is compensated by the size of EPE content (see Fig. 5) so that the timescale of the balance terms in the different layers is of the same magnitude, of order 100 days and thus comparable to timescales of frictional processes: the timescale of the bottom friction is $1/\epsilon \approx 100$ days, the time of nonlinear bottom friction and the timescale of the SGS parameterization, when taken for the grid scale, are of the same size. The timescale of the rates of energy conversion is clearly of the order of the frictional processes.

The timescales associated with balance rates of the QPV and thickness fluxes are in strong contrast to those of the scalar quantities. In Fig. 10 we compare the timescales of the terms of the QPV flux and thickness flux with some scaling laws explained below. More specifically, the times shown there are associated with the sink rate due to the ageostrophic terms in the flux balances,

$$\mathcal{T}_i = -\frac{\overline{v_i' q_i'}}{\mathcal{V}_i} \qquad \mathcal{T}_\eta = -\frac{\overline{v_2' \eta'}}{Q}, \tag{17}$$

evaluated at the channel center. The $\mathcal{T}_i$ differ by an order of magnitude in the layers and $\mathcal{T}_\eta$ is somewhat smaller than $\mathcal{T}_2$. In the bottom QPV flux and the thickness flux we find relaxation scales of the order of 10 days, and in the top layer $\mathcal{T}_1$ ranges from a few hours to a maximum of 1.5 days.

These times are certainly not associated with friction but must be internally established by the flow dynamics. To gain a view of the temporal behavior of the eddy field we have evaluated the covariance of the meridional eddy velocity at various places in the channel. Figure 9 shows the correlation functions for case EFB. Six years of data at five meridional positions (center, on the flanks of the jet, and 500 km away from, near the boundaries) have been used and a zonal average has also been performed by taking the mean over ten points on the same latitude. In the jet the correlation is seen to decrease fairly rapidly after a few days. The microscale of the correlation is roughly three days, the integral scale ranges from about ten days in the center to 50 to 80 days outside the jet closer to the walls where the flow is less disturbed by eddies. For larger lags we find a quasiperiodic behavior at a very low correlation level, expressing the subsequent passing of similar eddies. In turbulence theory these correlation timescales are associated with advection and "overturning" of the eddies ($L/\bar{u}_i$ and $L/(\overline{v'^2_i})^{1/2}$ are, indeed, of the order of days but clearly not less than a day). The eddy flow is highly correlated in the vertical, cross-correlations between v'_1 and v'_2 look similar to the correlations with a maximum of 0.8 to 0.9 at zero lag.

While $\mathcal{T}_2$ and $\mathcal{T}_\eta$ may correspond to the micro- or macroscale of the correlations this is certainly not true for $\mathcal{T}_1$. This discrepancy is also found when relations to dynamically defined time scales are sought. From the dynamical point of view the most important internal timescales are associated with the baroclinic instability. Following Eady (1949) and Phillips (1954) the growth rates of baroclinically unstable disturbances are described by the timescales

$$T_{\text{Eady}} = \frac{\lambda}{U} \qquad T_{\text{Phillips}} = \frac{1}{\sqrt{\beta U}}, \tag{18}$$

written here for the two-layer channel geometry.[3] The first ignores the presence of the planetary vorticity gradient and may therefore not be appropriate. Both apply strictly, of course, to the linear phase of baroclinic instability and, moreover, to horizontally constant shear. Values for T_{Eady} and T_{Phillips} are given in Table 2, with the shear evaluated at the center of the channel. They are of the order of a few days, the Eady timesscale being generally smaller than the Phillips timescale.

McWilliams et al. (1978) have determined the linear stability of the mean jet of their channel experiment and found a period of 9 days, which is in favor of the Phillips timescale.

The ratio of the timescales of the flux balances and the Phillips timescale, shown in Fig. 10 versus shear, exemplifies the fundamental problem of scaling. In general $\mathcal{T}/T_{\text{Phillips}}$ scatters about an average value by less than one order of magnitude, but this is roughly the range of the $\mathcal{T}$ or the Phillips timescale itself. Closer inspection, moreover, reveals clearly that within each group *FB (shown as *), *G4 (shown as ×) and *B5 (shown as +) of the experiments we see a decrease with shear, suggesting that further scaling by β and λ could possibly achieve a power law behavior of the ratio. Any additional scaling by β would affect only the level of the *B5 experiments and similarly, λ-scaling only affects the *G4 experiments. A reasonable power law scaling $\mathcal{T} \sim \beta^a \lambda^b U^c$ can easily be found, none, however, in a universal form with a nondimensional coefficient of proportionality, indicating dependence on scales that have not been considered in our experiments. We conclude that $\mathcal{T}_2$ and $\mathcal{T}_\eta$ are of the order of the baroclinic instability timescales but none of the above scalings (18) is successful.

4. Diffusive models

The main support for a diffusive form as a representation of the eddy induced flux of QPV or layer thickness, found in the EPE and EAPE balances, is the property of these fluxes to be downgradient of the corresponding mean quantities, despite the presence of significant fluxes by eddy-induced triple moments. There is a widespread agreement about a parameterization for the eddy fluxes of scalars (heat and passive tracers) as a diffusion of corresponding mean properties. The eddy flux of the active tracer QPV is often presented in a diffusive form as well (e.g., Welander 1973; Held 1975, 1978; Marshall 1981; Held and Hoskins 1985; Vallis 1988; Larichev and Held 1995; Pavan and Held 1996; Held and Larichev 1996; Treguier et al. 1997):

$$\overline{v_i' q_i'} = -k_i \frac{\partial \overline{q}_i}{\partial y}. \qquad (19)$$

Another prominent example of diffusive parameterization is the representation of the eddy-induced mass flux $\overline{v_i' \eta'}$ in isopycnal layers by a downgradient flux with respect to mean layer thickness,

$$\overline{v_1' \eta'} = \overline{v_2' \eta'} = -\kappa \frac{\partial \overline{\eta}}{\partial y}. \qquad (20)$$

This eddy flux is the effective transport velocity in isopycnal formulations of mean transport equations for tracers (see, e.g., Gent and McWilliams 1990; Gent et al. 1995). In the momentum balance (5) the lateral eddy mass transport is equivalent to a vertical momentum transport, and the parameterization (20) then implies vertical transport of horizontal momentum with a diffusion coefficient $\kappa(H_i/\lambda_i)^2$. In the layer framework this appears as interfacial friction. Notice that in truly large-scale flow where the respective contributions of relative vorticity can be neglected in the QPV flux, as well as the mean QPV gradient, the main difference between QPV diffusion and thickness diffusion is found in the presence of the eddy transport of planetary vorticity, $k_i\beta$, in (19). As demonstrated in section 2b both these conditions fail to apply to our experiments: in the upper layer the Reynolds stress cannot be neglected, in the lower layer the mean relative vorticity is significant.

a. QPV and thickness diffusivities

The values of the transfer coefficients k_i for QPV and κ for layer thickness are displayed in Fig. 11. They have been evaluated using zonal and time averages of the eddy fluxes and the mean gradients. The profiles of the QPV diffusivities are rather complex. A local minimum is observed in the jet center, while highest values are found on the flanks of the jet. The coefficients have different shapes in the layers and have a clear ordering of magnitude, $k_2 > k_1$. Relative to the maximum the valley in k_1 is deeper than in k_2. The cases show significant differences for different parameters of bottom friction, stratification and β, for example, in the width of the central valley and the height of the peaks above the valley, but clear parametrical dependences cannot be evaluated from such a limited suite of experiments. For the low β cases both k_i, and for the high friction cases, the k_2 diffusivity seem to settle on an almost constant shape in the jet region. The diffusivity for layer thickness has a simpler structure, which becomes more evident in the cases with higher friction: the diffusivity is more or less constant in the jet, starting to decrease in the region of the flanks.

Similar shapes for numerically determined diffusivities in a three-layer QG channel flow are reported by McWilliams and Chow (1981). Eddy-flux closure could not, however, stop with the knowledge of the positivity of coefficients. A physically motivated representation of their complex structure must be given. We discuss a few parameterizations and scaling theories that have been suggested to explain the shape and/or the overall size.

b. Parameterizations

All attempts known to us to parameterize the shape of the diffusivities k_i and κ have been performed in terms of algebraic functions of the local vertical shear U. We would like to emphasize, however, that there is no evidence for any single-valued relation between the diffusivities and the shear U in any of our experiments. As exemplified for EFB in Fig. 12, all cases yield multiple-valued relations. Notice, however, that this occurs predominantly in the flank region and not in the central jet.

Marshall's (1981) closure is written in the form $k_i \sim U$. It is based on Green's (1970) and Stone's (1972) form of the transfer coefficients for an infinitesimal wave growing linearly on a baroclinically unstable mean flow where the eddy transport coefficient of heat is proportional to the lateral gradient of the mean temperature or shear. Held (1978) has extended the Green–Stone concept to disturbances that do not fill the entire height of the fluid but are confined to a lower active portion. This yields a dependence $k_i \sim U^4$. Held and Pavan (1996) have recently suggested a parameterization for a wide jet. On the basis of numerical experiments similar to ours but driven by relaxation to a prescribed shear they find for sufficiently broad jets a parameterization $k_i \sim U^{3/2}(U - U_{\text{crit}})^{3/2}$ where $U_{\text{crit}} \approx \beta\lambda^2{}_2$ is the shear magnitude, which is critical for baroclinic instability. Ivchenko (1985b) pointed out that the Green–Stone closure scheme $k_i \sim U$ is inappropriate under strongly baroclinic conditions. He noticed that the minimum in the eddy diffusivities could be obtained in an expression placing the QPV gradient (with its central maximum) in the denominator. A more or less concentrated jet[4] can indeed be obtained with a diffusive parameterization of the form $k_i \sim U/(U^2 + U^2_0)$ with a free shape parameter U_0. This was tested by Wolff (1990), Sinha (1993), and Ivchenko et al. (1997). A peculiar property of this parameterization should be noted: for small U_0 that is, strongly baroclinic conditions, the transport of QPV is inversely proportional to the gradient of QPV, which contrasts the general concept of a diffusive process: though being downgradient, the transport of QPV is large where the gradient is small and vice versa. In an unforced initial value problem, such a flux leads to an unstable situation.

With exception for this last form (which still is physically not very sound) all these parameterizations fail to simulate the double peak structure of the coefficients and do not yield any substantial concentration of momentum in a jet. A detailed discussion of the failure of various similar forms of the Green–Stone parameterization for the thickness flux in a similar two-layer channel flow is found in McWilliams et al. (1978).

c. Scaling theories

The QPV diffusivity of the top layer is constrained in its magnitude by the momentum balance (5). The steady-state condition of this balance and the dominance of the stretching part of the mean QPV gradient leads to $k_1 \approx \tau\lambda^2{}_1/U$. Thus $k_1 \sim \lambda^2/U$, which, however, is not a parameterization. In the lower layer, and particularly for the thickness diffusion, the shape of the diffusivity could possibly be decoupled from its overall magnitude and thus, scaling could be successful. In particular the κ values show a clear ordering of magnitudes in Fig. 11.

From dimensional reasoning the diffusivity (QPV or thickness) can be represented in a mixing length form, $k \sim L^2/T \sim VL \sim TV^2$, with appropriate length, time, and velocity scales. The Green–Stone (GS) concept uses the Rossby radius λ supplemented by the Eady timescale T_{Eady}. In our case the Phillips timescale T_{Phillips} may be more appropriate. The diffusivities of these models take the form

$$k_{\text{Eady}} \sim \frac{\lambda^2}{T_{\text{Eady}}} = \lambda U$$

$$k_{\text{Phillips}} \sim \frac{\lambda^2}{T_{\text{Phillips}}} = \lambda^2\sqrt{\beta U}. \qquad (21)$$

Because the diffusive process operates over a scale L, which is certainly larger than λ (see, e.g., Stammer 1998) and correlation properties of the eddy field are not explicitly taken into account in the above expressions, there are

nondimensional coefficients in these relations that generally are not of order unity (see, e.g., Visbeck et al. 1997). Larichev and Held (1995) and Held and Larichev (1996) have recently suggested an alternative scaling model. Their scaling law (HL) is derived for fully developed homogeneous β-plane turbulence in the presence of a supercritical shear. They found that the eddy field will be made more barotropic and the inverse energy cascade will expand the eddy scales toward the barotropic Rhines scale, $L_R = (C/\beta)^{1/2}$ where C is the barotropic velocity (Rhines 1975). Then, with the scaling $C \sim \xi U$ obtained from energy balance considerations, where $\xi = U/(\beta\lambda^2)$ is the supercriticality,[5] and assuming a mixing length form with barotropic velocity and length scales, Held and Larichev arrive at the scaling law

$$k_{HL} \sim CL_R \sim \lambda U \xi^2 = \frac{L_R^2}{T_{\text{Eady}}}. \qquad (22)$$

As indicated in the last equality, the Rhines scale and Eady timescale are apparently working together in the *HL* scaling.

As an example of the diffusivity scaling we show in Fig. 13 the ratio of the diffusivities and the Eady scaling. All fields are evaluated at the channel center (for values see Table 2). As seen in Fig. 13 neither of k_2 or κ satisfies the GS scaling. Instead we find a decrease of the diffusivities with increasing shear, which is not as strong in case of k_1. As in case of the timescales considered above, a power law scaling $k \sim \beta^a \lambda^b U^c$ can be achieved, but there is no universal form without involving additional scales.

It is evident that this scaling is not appropriate, and similar negative results are obtained for the other scaling laws discussed above. We must conclude that the strong requirement of steady-state and zonal-mean condition and the hard constraint on the eddy QPV flux in top-layer momentum appears to make any scaling attempt of k_1 under these conditions meaningless. Because the Reynolds stress is introduced as a “free” mode of dynamics—it is largely free in terms of shape and magnitude—we have some freedom in the thickness flux and the lower-layer QPV flux but this concerns only the shape, not the overall (integrated) magnitude, which is again set by the wind stress.

We conclude this discussion of diffusive models with a negative statement: the conventional diffusive parameterizations and the scaling theories do not account for the complex structure of the QPV and thickness diffusivities. They fail to reproduce the double peak structure responsible for the concentration of zonal momentum in the jet. They also fail to adjust their magnitudes to any of the above presented scaling laws as consequence of the strong constraint imposed by the momentum balance of the system. We would like to note that more complexity in the model by adding more layers would not lead to a basically different conclusion. In a multilayer model as shown, for example, in Marshall et al. (1993, and there even with topography, realistic coast lines, and nonzonal wind stress) the momentum is constrained to be transferred essentially unchanged through the interior frictionless layers because Reynolds stress effects are negligible, as here in the bottom layer, and—because in a zonal mean flow with QG dynamics—there are no other transport mechanisms than interfacial stresses. This property implies that interfacial stresses in the interior would have to scale as the top and bottom layer thickness fluxes.

5. A parameterization derived from the QPV flux balance

The balances of the second-order moments are not under direct control of the constraint imposed by the balance of mean momentum. We investigate their usefulness for proving or disproving the existence of diffusive behavior for QPV and thickness transport by the eddies. We have identified dominant eddy induced fluxes by triple moments in the balances of the scalar second-order quantities and the eddy fluxes. Any consideration of these equations for the purpose of parameterization, going beyond the ascertainment of the positiveness of coefficients, must certainly face the task of handling the triple moments. We present a parameterization of the QPV flux derived from the balance of this flux and a special closure of the corresponding triple moment. This concept is easily transferred to a parameterization of the thickness flux.

Since the QPV flux is derived from a vector quantity, any theory involving the second-order moments must consider the flux balance. Our concept of using the QPV flux balance for parameterization of this flux is based upon the notion of a very simple and special form of balance: there is source of flux by a gradient term, redistribution by a geostrophic triple moment, and sink due the remaining imbalance representing the ageostrophic pressure-QPV covariance and the Coriolis term. Replacing the ageostrophic sinks by a relaxation term of the form (17) and ignoring the small Coriolis term here for simplicity we arrive at

$$\frac{\overline{v_i' q_i'}}{\mathcal{T}_i} = -\overline{v_i'^2}\frac{\partial \overline{q}_i}{\partial y} - \frac{\partial}{\partial y}\overline{v_i'^2 q_i'}, \qquad (23)$$

which allows a physically meaningful interpretation. We can identify a partly diffusive form of the flux with a diffusion coefficient $K_i = \mathcal{T}_i \overline{v_i'^2}$ and a correction term, which is not directly related to the mean gradient but results from the triple moment in the flux balance. As demonstrated in Fig. 8 the latter is actually a small contribution in the bottom layer but contributes in the top layer. The approach leading to (23) is similar to the situation of turbulence closure in convective boundary layers (see, e.g., the review by Lykossov 1995) where attempts are made to diagnose the vertical turbulent flux of heat from the heat flux balance. The turbulent pressure gradient–temperature covariance in this balance (corresponding basically to our ageostrophic terms) is traditionally associated with a relaxation process (Rotta 1951), as done here with the ageostrophic pressure–QPV covariance.

A similar approach can be applied to the balances of EPE and EAPE, relating eddy enstrophy and thickness variance to the gradients of QPV or layer thickness, respectively, and the corresponding second order eddy fluxes. As shown above, the timesscales involved in these relations are much longer than the timescale on which the QPV flux relaxes to the form given above.

a. Parameterization of the flux triple moment

The local relation between the flux and mean gradient in (23) may be based on a false pretense: the divergence of the triple moment $\overline{v_i'^2 q_i'}$ may introduce nonlocal behavior. A more precise treatment should also consider the weak coupling to the zonal flux explicitly. We proceed by searching for an advective closure of the triple moment that turns the QPV flux–gradient relation into a local form.

Breaking down the triple moment in the QPV flux balance, $\overline{v_i'^2 q_i'}$, into lower order moments the tensorial character of the moment must be preserved. It is a member of the tensor $\overline{\mathbf{u}_i' \mathbf{u}_i' q_i'}$, so we try the form

$$\overline{v_i'^2 q_i'} = \overline{v_i'^2}\,\overline{\omega}_i. \qquad (24)$$

There are not very many possible candidates for the pseudoscalar $\overline{\omega}_i$. In Fig. 14 we give examples of a regression fit of (24) using the mean relative vorticity,

$$\overline{\omega}_i = -\gamma_i \nabla^2 \overline{\psi}_i = \gamma_i \frac{\partial \overline{u}_i}{\partial y}, \qquad (25)$$

with a dimensionless coefficient γ_i to the "data" of the triple moment from the numerical experiments. The fit with constant coefficient γ_i works quite well. The rms between the triple moment "data" and the fitted functionals indicates a misfit of roughly 10% to 30% and the values for the γ_i have an overall consistent pattern of size and sign within all cases. Other such simple choices for the pseudoscalar factor $\overline{\omega}_i$ can hardly be given (the mean QPV, the planetary or stretching, vorticities do not work). It should be noted that the other components of the tensor $\overline{\mathbf{u}_i' \mathbf{u}_i' q_i'}$ can be represented by closures corresponding to (24) and (25).

b. Parameterization of the QPV flux

Using (24) and (25) the QPV flux balance appears in the parameterized form

$$\begin{aligned} \overline{v_i' q_i'} &= -K_i \frac{\partial \overline{q}_i}{\partial y} + \gamma_i \mathcal{T}_i \frac{\partial}{\partial y}[\overline{v_i'^2} \nabla^2 \overline{\psi}_i] \\ &= -K_i \frac{\partial}{\partial y}[\overline{q}_i - \gamma_i \nabla^2 \overline{\psi}_i] + \gamma_i \mathcal{T}_i \nabla^2 \overline{\psi}_i \frac{\partial}{\partial y} \overline{v_i'^2} \end{aligned} \qquad (26)$$

with $K_i = \mathcal{T}_i \overline{v_i'^2}$. It is determined by one free constant parameter γ_i, a diffusivity K_i, and either the timescale $\mathcal{T}_i$ of the QPV flux relaxation or the covariance $\overline{v_i'^2}$. These latter quantities must still be considered to be a function of position. Below we argue that the term involving the derivative of the covariance is small in our experiments and that K_i can be

considered constant in the jet region. A coarse model is then developed with two constant parameters in each layer. A more general model based on (26) in a complete second-order closure approach would, however, require additional equations or recipes to determine γ_i, K_i and either of $\mathcal{T}$ or $\overline{v_i'^2}$.

Comparison of the two γ_i terms in (26) shows for all experiments that $\overline{v_i'^2}\,\partial\nabla^2\overline{\psi}_i/\partial y$ is always smaller than $(\partial\overline{v_i'^2}/\partial y)\nabla^2\overline{\psi}_i$ (by a factor of roughly 0.2), indicating that the meridional scale of the jet must be smaller than the scale of the covariance. But also, the vanishing of relative vorticity and the derivative of covariance in the center of the jet helps to establish this result. In the following we abandon the second γ_i term to describe a simple shortcut of parameterization.

The concept to express all deviations from a homogeneous state (where $\gamma_i = 0$) by the correction term only makes sense if the resulting diffusivity has a simple, almost constant shape. Ignoring the last term in (26) we use in Fig. 15 this relation in the form

$$-\overline{v_i' q_i'} \Big/ \frac{\partial \overline{q}_i}{\partial y} = k_i = K_i\left[1 + \gamma_i \frac{\partial^2 \overline{u}_i}{\partial y^2} \Big/ \frac{\partial \overline{q}_i}{\partial y}\right] \qquad (27)$$

to compare the numerically determined QPV flux—in the form of the k_i—with the expression on the rhs. The structure resulting from fitting the rhs of (27) with constant γ_i and K_i is displayed by the dashdotted curve and the values of these coefficients are given in Table 3. It is clearly seen in Fig. 15 that the γ_i term compensates for the double peak structure of k_i. Notice that in the top layer the fitted curve and the k_1 lie almost on top of each other; for the deep layer there is good agreement in the entire "valley" region of k_2. The coefficient K_i can thus indeed be considered constant over the entire jet region.

We have attempted a scaling of the diffusivity K_i by the scaling laws discussed in section 4c but obtained similar negative results as for the QPV diffusivities. In the present state of this work the K_i as well as the γ_i must be taken without a universal basis. The values of the γ_i in Table 3 clearly show that the correction to conventional QPV diffusion is most important in the top layer where the contribution of the relative vorticity gradient to the QPV gradient is even overcompensated:the correction affects a change of sign of the contribution from the relative vorticity. In the bottom layer the correction is generally small.

c. A closed coarse model

Neglecting the last term in the parameterization (26) the steady state momentum balance (5) becomes

$$-K_1\left[(\gamma_1 - 1)\frac{\partial^2 \overline{u}_1}{\partial y^2} + \frac{f_0^2}{g^* H_1}(\overline{u}_1 - \overline{u}_2) + \beta\right] + \frac{\tau_1}{H_1} = 0$$

$$-K_2\left[(\gamma_2 - 1)\frac{\partial^2 \overline{u}_2}{\partial y^2} - \frac{f_0^2}{g^* H_2}(\overline{u}_1 - \overline{u}_2) + \beta\right] - \epsilon \overline{u}_2 = 0. \qquad (28)$$

Though any parameterization of the complete QPV flux cannot consider lateral transport and vertical exchange of momentum in separation, the above equations suggest a simple interpretation in terms of these processes. The contribution arising from the relative vorticity describes lateral transport and the stretching part contains the vertical exchange of momentum between layers. The β term is a source of eastward momentum due to the mere presence of eddies (i.e., nonzero K_i). It appears similar to the Neptune effect investigated by Holloway (1992);a physical interpretation is, however, not easily found. The considerations outlined below suggest to combine the stretching part and the β term in a particular way to enable an interpretation by eddy-induced interfacial friction and a direct driving of the flow by eddies.

Because the diffusivities K_1 and K_2 differ, the stretching part of the QPV gradient in the two layers cannot entirely be

attributed to momentum exchange. This part is split apart by rewriting (28) in the form

$$-K_1(\gamma_1 - 1)\frac{\partial^2 \overline{u}_1}{\partial y^2} - \frac{K_1 + K_2}{2\lambda_1^2}U + \frac{K_2 - K_1}{2\lambda_1^2}[U - U_1^{\text{crit}}]$$

$$+ \frac{\tau_1}{H_1} = 0$$

$$-K_2(\gamma_2 - 1)\frac{\partial^2 \overline{u}_2}{\partial y^2} + \frac{K_1 + K_2}{2\lambda_2^2}U + \frac{K_2 - K_1}{2\lambda_2^2}[U - U_2^{\text{crit}}]$$

$$- \epsilon \overline{u}_2 = 0, \qquad (29)$$

where $U = \overline{u}_1 - \overline{u}_2$ and $\lambda^2_i = g^* H_i / f^2_0$ as before, and

$$U_i^{\text{crit}} = \beta \lambda_i^2 \frac{2K_i}{K_2 - K_1}. \qquad (30)$$

The first part of the stretching term in (29) represents momentum exchange between the layers; it has the form of interfacial friction. Because $K_2 - K_1 > 0$ in all our experiments and thus $U^{\text{crit}}_i > 0$ as well, the second part of the stretching term in (29) represents a source of eastward momentum where the shear exceeds the corresponding critical value U^{crit}_i; at other places the flow is retarded.

In comparison to conventional QPV diffusion the most important feature of the coarse model (29) is the direction of the lateral momentum transport by the diffusive term. It is controlled by the parameter γ_i. If $\gamma_i = 0$, we are facing the conventional QPV diffusion parameterization where momentum is transferred downward the lateral velocity gradient (pure QPV diffusion with consideration of the relative vorticity implies diffusion of momentum, i.e., downgradient diffusive transfer). With $\gamma_2 > 1$ and $\gamma_1 < 0$, as found in our experiments, the correction term in the parameterization (26) causes a countergradient transfer of momentum in the upper layer and a stronger downgradient transport in the lower layer. Both these processes thus cause an increase in shear. Remember that this property results from the triple moment in the QPV flux balance.

The direct eddy driving causes as well an increase of shear if $U^{\text{crit}}_2 > U > U^{\text{crit}}_1$, as in our experiments. The separation of the QPV gradient thus leads to a momentum balance of the jet where interfacial friction is the only sink of eastward momentum in the top layer and the only source in the bottom layer.

The model has to consider the integral constraint (8). Using the present parameterization of the QPV flux the constraint becomes

$$\frac{1}{2}\int_{-Y/2}^{Y/2} (K_2 - K_1)U \, dy$$

$$= \sum_{i=1}^{2} \int_{-Y/2}^{Y/2} \lambda_i^2 K_i \left[\beta + (\gamma_i - 1)\frac{\partial^2 \overline{u}_i}{\partial y^2}\right] dy. \qquad (31)$$

It may be satisfied by reducing the number of coefficients. In the regime of our experiments the last term on the rhs is small compared to the (positive) first. Hence, in case of eastward flow where $\tau_1 > 0$ we have $U > 0$, and thus $K_2 > K_1$ is required at least in part of the domain. In a westward forced flow where $\tau_1 < 0$ and $U < 0$ we find the condition $K_2 < K_1$, as described by Ivchenko et al. (1997) for an experiment of our channel model with westward forcing.

With constant coefficients (28) can be solved analytically.[6] The relative vorticity term introduces two lateral scales that are independent of the forcing scale. In case of conventional QPV diffusion (i.e., $\gamma_i = 0$) these scales are the Rossby radius $\Lambda_1 = \lambda$ and a scale $\Lambda_2 = [(K_2/\epsilon)(H_1 + H_2)/H_2]^{1/2}$, which results from the balance of diffusion and friction in the bottom layer. Modifications of the sinusoidal behavior of the forcing only occurs in boundary layers at the walls. As shown in Fig. 16 (upper left panel) the exponential boundary layer penetrates quite far into the interior (in this example we have $\Lambda_2 \approx$ 200 km $\gg \lambda$) and mimics a sharpening of the jet. In a broader channel this would not occur but the central jet would still be sinusoidal as the forcing. The countergradient transport arising from the triple correction switches the boundary layer behavior to a radiating behavior [both eigenvalues of the linear operator on the lhs of (28) change sign]. Figure 16 (lower-left panel) shows the effect of the correction term: the central jet is concentrated and intensified flanks occur as in the numerical experiments (compare with Fig. 2). The left panels of the figure consider the resulting profiles for an f plane where the solution with constant diffusivity and homogeneous boundary condition on $\bar{u}_i$ is purely sinusoidal.

6. Summary and conclusions

In a β-plane channel the wind stress drives an unstable eastward flow in which eddies in the top layer generate a Reynolds stress, which is convergent over the central region. It causes a narrow supercritical jet with a meridional scale much smaller than the scale of the wind stress but larger than the baroclinic Rossby radius. The downward transfer of momentum by the eddy-induced interfacial form stress feeds on the Reynolds stress convergence and drives a deep jet against the bottom friction.

The two-layer model of wind-driven quasigeostrophic flow in a zonal channel has long been in use for studying the dynamics of large-scale oceanic currents, in particular when eddy effects have been addressed. The first eddy-resolving numerical models of the Antarctic Circumpolar Current were based on this model (e.g., McWilliams et al. 1978), and conventional diffusive parameterizations derived from the theory of baroclinically unstable waves (e.g., Green 1970; Stone 1972) were tested (e.g., Marshall 1981) to motivate closed coarse models of the eddy-effected mean flow. A second line of research on two-layer QG dynamics stems from the atmospheric community studying homogeneous turbulence on a β plane in the presence of a vertical shear and advocating a diffusive form for the eddy-induced transport of QPV. However, the conditions of the homogeneous model (e.g., Vallis 1988; Held and Larichev 1996), where Reynolds stresses and the mean currents are laterally uniform, are not realized in the regime of our wind-driven flows. In the flow of the present study there is a significant Reynolds stress divergence in the top layer and the relative vorticity of the mean flow is not negligible.

We have extended the analysis of the wind-driven flow regime to include the balances of second-order moments, namely eddy potential enstrophy, eddy energies, and the QPV flux, in order to test proposed parameterizations of eddy fluxes of QPV and layer thickness. The second-order balances confirm the well-known properties of the direction of the eddy fluxes in relation to the relevant mean gradients: the Reynolds stress is upgradient and the fluxes of QPV and layer thickness are downgradient. These properties correspond to the Lorenz cycle of a baroclinically unstable regime but what is clearly revealed here—and lost in the integrated form as shown, for example, in McWilliams et al. (1978)—is that all second-order balances contain significant contributions from eddy transfer by triple moments. A second important property of the balances is found in the magnitude of the timescales of the balance rates. While the scalar moment enstrophy and energies relax on time scales $O(100)$ days, as dictated by frictional effects, the balance of the fluxes reveals a very strong relaxation within a few days, even less than a day in top layer. These time scales can roughly be associated with the linear growth rates of baroclinic instability but convincing regressions between the times scales of flux production and destruction could not be found. The difference of top and bottom layer timescales in the flux balances has a correspondence in the level of eddy activity seen in the eddy energies and enstrophies. The deep layer is in a much weaker eddy state than the top layer.

Diffusivities for QPV and layer thickness, determined from the numerical experiments, cannot be reproduced by any of the known parameterizations of eddy fluxes, as those derived for infinitesimal growing unstable waves (Green 1970; Stone 1972) or those derived from the homogeneous model (e.g., Pavan and Held 1996). The double peak shape of the QPV diffusivities cannot, at all, be parameterized by a single-valued functional of the vertical shear. Layer thickness diffusivities have a simpler form, more or less constant in the jet range. Neither of them, however, follows the magnitude scaling derived from Green–Stone or Held–Larichev scaling laws. Conventional diffusive transport of QPV or thickness thus fails in the wind-driven regime. This failure is explained, in the first place, by the necessity that the fluxes have to satisfy the balance of zonal momentum, which dictates their level and to a large degree also their form. The existence of significant triple moment divergences in the second-order balances also contributes to this failure.

Eddy flux closure for quasigeostrophic flows has been conceived on the basis of the balance of eddy potential enstrophy. Under the assumption that the eddy-induced transport of enstrophy is negligible, support of diffusive downgradient parameterizations has been taken (e.g., Shutts 1983; Treguier et al. 1997) and it was also suggested—as a consequence of this balance—that the eddy QPV flux must be intimately related to the enstrophy dissipation (e.g., Held and Hoskins 1985). We propose, on the contrary, that the scalar balances—eddy enstrophy and potential energy—only reflect the flux direction in terms of mean gradients but that parameterizations are more severely constrained by the balances of fluxes themselves

which, as pointed out above, are subject to a very fast adjustment.

The balances of QPV flux and of thickness flux have a very simple form. Flux is created by a gradient term proportional to either mean QPV or thickness gradient, and destruction of flux is achieved by the covariance between the ageostrophic pressure and the eddy QPV or interface displacement, respectively. Other terms in the flux balances are small with the exception of the triple moment divergence in the top layer. We suggest replacing the ageostrophic pressure covariance by a flux damping term, as in Rotta's (1951) approach to turbulence closure. The resulting flux balance allows expressing the flux as a sum of downgradient diffusion plus corrections from triple moments and possibly other small terms in the flux balance. The diffusivity takes a mixing length form; it is the product of the damping timescale and the eddy velocity covariance. In this framework the eddy fluxes are not directly related to any dissipation terms but result in a fast adjustment process between gradient production and pressure correlations.

The QPV and thickness flux balances clearly show that fluxes are not only caused by the mean gradients but also by other terms in the flux balances. According to our experiments the triple moment is by far the largest contribution after the mean gradient term. For practical utilization of the new form of parameterization of second-order fluxes it is necessary to break down the triple moments into lower order moments. We have found a simple and effective parameterization in terms of velocity variance and mean vorticity that explains the shape of the triple moments in the flux balances of all experiments (with one free coefficient per layer, varying for the different experiments). Combining the damping form of the flux balance with the parameterized triple moment yields, as final result of this paper, a parameterization of the QPV or thickness flux. The parameterized QPV flux is finally used in a simple steady coarse model of momentum transfer with constant diffusivities. It reproduces the jet structure in a consistent way.

There are many issues to be clarified in this new approach. The parameterization of the eddy flux of QPV contains two coefficients for each layer. It is not clear how these should be determined without a high resolution experiment as support and without any satisfying scaling theory. One of these—the coefficient of the triple moment correction term—can quite safely be considered constant. In our simple model we have taken the diffusivity as constant. The fitted diffusivities, however, still show a weak dependence on the lateral coordinate outside the jet region, which might be important and must then be replaced by a parameterized form in terms of lower order quantities. A refined theory is still needed to determine the diffusivities and other parameters of the present model from a more complete second-order closure approach.

Another issue is the applicability of the coarse model to conditions more general than the quite constrained QG channel flow in two layers considered here. Even more important is the implementation in circulation models that are not governed by QG equations. Considering a higher vertical resolution but still retaining QG dynamics, we propose as an extrapolation of our findings that the triple moment correction of the QPV flux is only important in the top "boundary" layer and that the deeper layers are governed by conventional QPV diffusion. The role of the correction terms is then seen in the "extra" convergence of momentum, which structures the jet in the upper layer and feeds this structure into the lower layers by the vertical transport of momentum via the interfacial friction mechanism discussed in section 5c.

Acknowledgments

We like to thank our colleagues Vladimir Ivchenko, Vladimir Gryanik, and Dimitrii Mironov for many discussions and helpful suggestions.

REFERENCES

Andrews, D. G., J. R. Holton, and C. B. Leovy, 1987: *Middle Atmosphere Dynamics.* Academic Press, 489 pp..

Arakawa, A., 1966: Computational design for long term numerical integration of the equations of fluid motion: Two-dimensional incompressible flow. Part I. *J. Comput. Phys.,* **1,** 119–143..

Böning, C. W., and F. O. Bryan, 1996: Large-scale transport processes in high-resolution circulation models. *The Warmwatersphere of the North Atlantic Ocean,* W. Krauss, Ed., Gebr. Borntraeger, 91–128..

Bretherton, F. P., 1966: Critical layer instability in baroclinic flows. *Quart. J. Roy. Meteor. Soc.,* **92,** 325–334..

Bryan, K., and L. J. Lewis, 1979: A water mass model of the World Ocean. *J. Geophys. Res.,* **84,** 2503–2517..

— ,J. K. Dukowicz, and R. D. Smith, 1999: On the mixing coefficients in the parameterization of bolus velocity. *J. Phys. Oceanogr.,* **29,** 2442–2456.. Find this article online

Danabasoglu, G., J. C. McWilliams, and P. R. Gent, 1994: The role of mesoscale tracer transports in the global ocean circulation. *Science,*

262, 1123–1126..

Eady, E. T., 1949: Long waves and cyclone waves. *Tellus,* **1,** 33–52..

England, M. H., 1993: Representing the global-scale water masses in ocean general circulation models. *J. Phys. Oceanogr.,* **23,** 1523–1552.. Find this article online

Gent, P. R., and J. C. McWilliams, 1990: Isopycnal mixing in ocean circulation models. *J. Phys. Oceanogr.,* **20,** 150–155.. Find this article online

— ,J. Willebrand, T. J. McDougall, and J. C. McWilliams, 1995: Parameterizing eddy-induced tracer transports in ocean circulation models. *J. Phys. Oceanogr.,* **25,** 463–474.. Find this article online

Green, J. S. A., 1970: Transfer properties of the large-scale eddies and the general circulation of the atmosphere. *Quart. J. Roy. Meteor. Soc.,* **96,** 157–185..

Held, I. M., 1975: Momentum transport by quasi-geostrophic eddies. *J. Atmos. Sci.,* **32,** 1494–1497.. Find this article online

— ,1978: The vertical scale of an unstable baroclinic wave and its importance for eddy heat flux parameterizations. *J. Atmos. Sci.,* **35,** 572–576.. Find this article online

— ,and B. J. Hoskins, 1985: Large-scale eddies and the general circulation of the troposphere. *Advances in Geophysics,* Vol. 28A, Academic Press, 3–31..

— ,and V. D. Larichev, 1996: A scaling theory for horizontally homogeneous, baroclinically unstable flow on a beta plane. *J. Atmos. Sci.,* **53,** 946–952.. Find this article online

Holland, W. R., and D. B. Haidvogel, 1980: A parameter study of the mixed instability of idealized ocean currents. *Dyn. Atmos. Oceans,* **4,** 185–215..

Holloway, G., 1992: Representing topographic stress for large-scale ocean models. *J. Phys. Oceanogr.,* **22,** 1033–1046.. Find this article online

Ivchenko, V. O., 1984: On the parameterization of the eddy fluxes of quasigeostrophic potential vorticity in zonal currents. *Dokl. Acad. Sci., USSR,* **277** (4), 972–976..

— ,1985a: On the parameterization of the eddy flows of geostrophic potential vorticity in zonal ocean currents. *Izv. Atmos. Oceanic Phys.,* **21** (8), 660–664..

— ,1985b: Parameterization of eddy momentum exchange in zonal flows. *Morsk. Gidrofiz. Z.,* **5,** 47–52..

— ,K. J. Richards, B. Sinha, and J.-O. Wolff, 1997: Parameterization of meso-scale eddy fluxes in zonal ocean flows. *J. Mar. Res.,* **55,** 1127–1162..

Killworth, P. D., 1997: On the parameterization of eddy transfer. Part I: Theory. *J. Mar. Res.,* **55,** 1171–1197..

Large, W. G., J. C. McWilliams, and S. C. Doney, 1994: Oceanic vertical mixing: A review and a model with nonlocal boundary layer parameterization. *Rev. Geophys.,* **32** (4), 363–403..

Larichev, V. D., and I. M. Held, 1995: Eddy amplitudes and fluxes in a homogeneous model of fully developed baroclinic instability. *J. Phys. Oceanogr.,* **25,** 2285–2297.. Find this article online

Lykossov, V., 1995: Turbulence closure for the boundary layer with coherent structures: An overview. Ber Fachbereich Physik, Alfred-Wegener-Institut, Vol. **63,** 27 pp..

Maier-Reimer, E., U. Mikolajewicz, and K. Hasselmann, 1993: Mean circulation of the Hamburg LSG OGCM and its sensitivity to the thermohaline surface forcing. *J. Phys. Oceanogr.,* **23,** 731–757.. Find this article online

Marshall, J. C., 1981: On the parameterization of geostrophic eddies in the ocean. *J. Phys. Oceanogr.,* **11,** 257–271.. Find this article online

— ,D. Olbers, H. Ross, and D. Wolf-Gladrow, 1993: Potential vorticity constraints on the dynamics and hydrography in the Southern Ocean. *J. Phys. Oceanogr.,* **23,** 465–487.. Find this article online

McDougall, T. J., and P. C. McIntosh, 1996: The temporal-residual-mean velocity. Part I: Derivation and the scalar conservation equations. *J. Phys. Oceanogr.,* **26,** 2653–2665.. Find this article online

McWilliams, J. C., 1977: A note on a consistent quasigeostrophic model in a multiply connected domain. *Dyn. Atmos. Oceans,* **1,** 427–441..

— , and J. H. S. Chow, 1981: Equilibrium geostrophic turbulence. I A reference solution in a beta-plane channel. *J. Phys. Oceanogr.*, **11,** 921–949.. Find this article online

— , W. R. Holland, and J. H. S. Chow, 1978: A description of numerical Antarctic Circumpolar Currents. *Dyn. Atmos. Oceans,* **2,** 213–291..

Pavan, V., and I. M. Held, 1996: The diffusive approximation of eddy fluxes in baroclinically unstable jets. *J. Atmos. Sci.*, **53,** 1262–1272.. Find this article online

Phillips, N. A., 1954: Energy transformations and meridional circulations associated with simple baroclinic waves in a two-level, quasi-geostrophic model. *Tellus*, **6,** 273–286..

Rhines, P. B., 1975: Waves and turbulence on a beta-plane. *J. Fluid Mech.*, **69,** 417–443..

Rix, N. H., and J. Willebrand, 1996: Parameterization of mesoscale eddies as inferred from a high-resolution circulation model. *J. Phys. Oceanogr.*, **26,** 2281–2285.. Find this article online

Rotta, J. C., 1951: Statistische Theorie nichthomogener Turbulenz. *Z. Phys.*, **129,** 557–572..

Semtner, A. J., and R. M. Chervin, 1992: Ocean general circulation from a global eddy-resolving model. *J. Geophys. Res.*, **97,** 5493–5550..

Shutts, G. J., 1983: The propagation of eddies in diffluent jetstreams:Eddy vorticity forcing of “blocking” flow fields. *Quart. J. Roy. Meteor. Soc.*, **109,** 737–761..

Sinha, B., 1993: The influence of mesoscale eddies and topography on Southern Ocean flows. Ph.D. thesis, University of Southampton, 197 pp..

Stammer, D., 1998: On eddy characteristics, eddy transports, and mean flow properties. *J. Phys. Oceanogr.*, **28,** 727–739.. Find this article online

Stone, P. H., 1972: A simplified radiative–dynamical model for the static stability of rotating atmospheres. *J. Atmos. Sci.*, **29,** 405–418.. Find this article online

Treguier, A. M., I. M. Held, and V. D. Larichev, 1997: On the parameterization of quasigeostrophic eddies in primitive equation ocean models. *J. Phys. Oceanogr.*, **27,** 567–580.. Find this article online

Vallis, G. K., 1988: Numerical studies of eddy transport properties in eddy-resolving and parameterized models. *Quart. J. Roy. Meteor. Soc.*, **114,** 183–204..

Visbeck, M., J. Marshall, T. Haine, and M. Spall, 1997: Specification of eddy transfer coefficients in coarse-resolution ocean circulation models. *J. Phys. Oceanogr.*, **27,** 381–402.. Find this article online

Welander, P., 1973: Lateral friction in the ocean as an effect on potential vorticity mixing. *Geophys. Fluid Dyn.*, **5**(1), 101–120..

Wolff, J.-O., 1990: Zur Dynamik des Antarktischen Zirkumpolarstroms. Ph.D. thesis, Universität Hamburg, 137 pp..

— , and D. J. Olbers, 1989: The dynamical balance of the Antarctic Circumpolar Current studied with an eddy resolving quasigeostrophic model. *Mesoscale/Synoptic Coherent Structures in Geophysical Turbulence*, J. C. J. Nihoul and B. M. Jamart, Eds., Elsevier Science, 435–458..

— , E. Maier-Reimer, and D. J. Olbers, 1991: Wind-driven flow over topography in a zonal β-plane channel: A quasigeostrophic model of the Antarctic Circumpolar Current. *J. Phys. Oceanogr.*, **21,** 236–264.. Find this article online

— , A. V. Klepikov, and D. J. Olbers, 1993: On the eddy potential enstrophy balance in a two-layer quasi-geostrophic channel model. *Ocean Modelling* (unpublished manuscripts), **101,** 3–5..

Tables

Table 1. Some integral quantities of the numerical experiments. The first two columns give the transport in the layers: $E^{\mathrm{kin}}{}_i$ and E^{pot} are the kinetic and available potential energies of the mean flow, andE'[cmi[cm$^{\mathrm{kin}}$ and E'^{pot} are the energies of the eddy

field.

	Transport		Energies					
Expt	Top (10^6 m^3 s^{-1})	Bottom (10^6 m^3 s^{-1})	$\overline{E}_1^{kin}$ (m^3 s^{-2})	$\overline{E}_2^{kin}$ (m^3 s^{-2})	$\overline{E}^{pot}$ (m^3 s^{-2})	$E_1'^{kin}$ (m^3 s^{-2})	$E_2'^{kin}$ (m^3 s^{-2})	E'^{pot} (m^3 s^{-2})
EFB	377	949	41	80	672	21	13	28
EG4	460	949	65	89	960	49	27	56
EB5	325	951	31	72	290	15	10	23
DFB	248	473	16	19	620	22	10	31
DG4	351	476	34	21	1703	47	18	114
DB5	206	475	11	17	267	16	7	26
NFB	276	599	19	27	609	23	12	31
NG4	350	522	32	24	896	47	20	54
NB5	246	648	15	28	248	17	9	26
HFB	340	862	31	57	613	22	13	29
HG4	405	762	46	53	909	45	23	51
HB5	315	930	25	58	250	16	10	25

Click on thumbnail for full-sized image.

Table 2. Parameters of the diffusivity scaling for all experiments:Rossby radius λ, Rhines scale L_R, barotropic and baroclinic velocities C and U, supercriticality $\xi = U/(\beta\lambda^2)$, Eady and Phillips timescales [see Eq. (18)]. All values are taken at the center latitude.

Expt	λ (km)	L_R (km)	C (m s^{-1})	U (m s^{-1})	ξ	T_{Eady} (days)	$T_{Phillips}$ (days)
EFB	32	193	0.43	0.18	15.3	2.1	8.2
EG4	45	206	0.49	0.30	12.9	1.7	6.3
EB5	32	251	0.36	0.11	19.5	3.3	14.4
DFB	32	134	0.20	0.13	11.1	2.9	9.6
DG4	45	152	0.26	0.25	10.8	2.1	6.8
DB5	32	170	0.17	0.07	13.0	4.9	17.7
NFB	32	132	0.20	0.11	9.5	3.3	10.3
NG4	45	147	0.25	0.23	9.9	2.3	7.2
NB5	32	176	0.18	0.06	11.2	5.7	19.0
HFB	32	164	0.31	0.13	11.7	2.7	9.3
HG4	45	177	0.36	0.25	10.9	2.1	6.8
HB5	32	217	0.27	0.08	13.5	4.7	17.3

Click on thumbnail for full-sized image.

Table 3. Result of fitting the parameterization (27) with constant $+\gamma$-$_i$ and K_i (in units of m^2 s^{-1}). For the fit of the two parameters special weight is given to the jet region. The resulting γ_i differ from those obtained from the triple moment fit (25) only slightly.

Expt	γ_1	γ_2	K_1	K_2
EFB	2.85	−0.225	1070	4340
EG4	3.2	−0.11	1220	7640
EB5	3.98	−0.328	1720	4510
DFB	3.45	−0.26	1090	4190
DG4	3.11	−0.84	1290	7650
DB5	2.71	−0.239	1710	4380
NFB	2.85	−0.157	1110	4460
NG4	2.86	−0.152	1240	7910
NB5	2.9	−0.127	1220	8520
HFB	3.54	−0.226	1110	4770
HG4	1.12	−0.241	1810	4890
HB5	3.5	−0.311	1810	5170

Click on thumbnail for full-sized image.

Figures

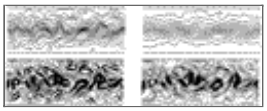

Click on thumbnail for full-sized image.

Fig. 1. Instantaneous (upper panels) and eddy streamfunctions (lower panels) for EFB; the upper layer is left and the lower layer is right. Contour intervals are 2×10^4 m^2 s^{-1} for the upper panels and 5×10^3 m^2 s^{-1} for the lower-left panel and 2.5×10^3 m^2 s^{-1} for the lower-right panel.

Click on thumbnail for full-sized image.

Fig. 2. Time and zonal mean profiles of the velocities $\bar{u}_i$ (full), the barotropic velocity $(H_1\bar{u}_1 + H_2\bar{u}_2)/(H_1 + H_2)$ (dash-dotted) and the vertical shear $U = \bar{u}_1 - \bar{u}_2$ (dotted) for EFB, DFB, NFB, and HFB as function of the scaled latitude y/Y. The critical phase speed $\beta\lambda^2_2$ is included as a straight line. Units are meters per second.

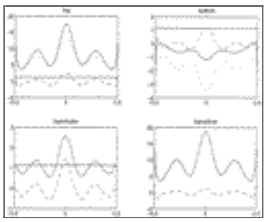

Click on thumbnail for full-sized image.

Fig. 3. The relative, stretching, and planetary part of the mean potential vorticity gradient for EFB as a function of the scaled latitude y/Y. Total gradient of QPV (full), relative part (dash-dotted), stretching part (dotted), and planetary part (full straight line). Units are 10^{-11} m^{-1} s^{-1}.

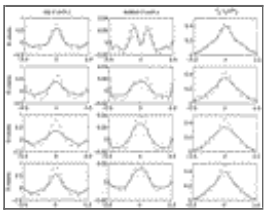

Click on thumbnail for full-sized image.

Fig. 4. Divergence of the Reynolds stress (left and middle panels) and the interfacial form stress (right panels) as function of the scaled latitude y/Y in units of 10^{-7} m s^{-2}. The divergence of the interfacial stress is presented here for the bottom layer (the top one is derived by multiplying with $-H_2/H_1$). Cases *FB (full), *G4 (dash-dotted), and *B5 (dotted).

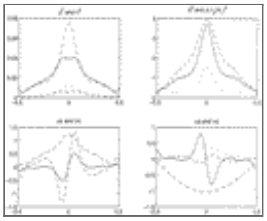

Click on thumbnail for full-sized image.

Fig. 5. Some second order fields for EFB. Velocity variances (upper-left panel): $\overline{u_1'^2}$ (full), $\overline{u_2'^2}$ (dashed), $\overline{v_1'^2}$ (dash-dotted), and $\overline{v_2'^2}$ (dotted). QPV and thickness variances (upper-right panel): $\overline{q_1'^2}$ (full), $100 \times \overline{q_2'^2}$ (dashed), and $(f_0/H_1)^2\overline{\eta'^2}$ (dotted). Thickness fluxes (lower-left panel):$0.1 \times \overline{u_1'\eta'}$ (full), $\overline{u_2'\eta'}$ (dashed), and $\overline{v_1'\eta'} = \overline{v_2'\eta'}$ (dash-dotted). QPV fluxes (lower-right panel): $0.1 \times \overline{u_1'q_1'}$ (full), $\overline{u_2'q_2'}$ (dashed), $\overline{v_1'q_1'}$ (dash-dotted), and $\overline{v_2'q_2'}$ (dotted) Units: velocity variances m^2 s^{-2}, QPV variance 10^{-10} s^{-2}, thickness fluxes m^2 s^{-1}, and QPV fluxes 10^{-7} m s^{-2}.

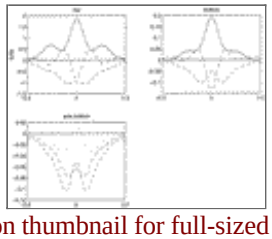

Click on thumbnail for full-sized image.

Fig. 6. Zonal and time-mean eddy enstrophy balance for EFB as a function of the scaled latitude y/Y, upper layer (upper-left panel), and lower layer (upper-right panel). The curves give the production (full), the eddy induced redistribution (dash-dotted), and the sink term $\overline{q_i'F_i'}$ in the EPE balance. The lower left panel displays the SGS part (dash-dotted) and resolved eddy part (dotted) of the sink term $\overline{q_2'F_2'}$ (dashed). Units are 10^{-14} m s^{-3}.

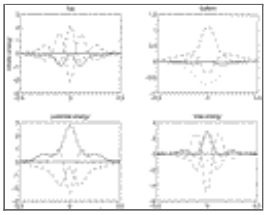

Click on thumbnail for full-sized image.

Fig. 7. Zonal and time-mean eddy kinetic and potential energy balances for EFB. The curves give the exchange with the mean flow energy (full), the eddy induced geostrophic redistribution (dash-dotted), the ageostrophic terms (dashed), and bottom friction (dotted). The total energy balance combines all gradient terms (full), all ageostrophic terms (dashed) and all geostrophic redistribution terms (dash-dotted) from both layers, the bottom friction term is dotted. Units are 10^{-5} m^3 s^{-3}.

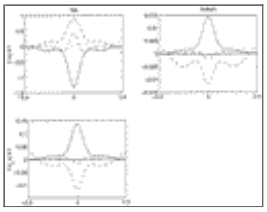

Click on thumbnail for full-sized image.

Fig. 8. Zonal and time-mean balance of the meridional QPV flux (upper panels) and thickness flux (lower panel) for EFB. Mean gradient term (full), Coriolis term (dotted), eddy induced redistribution (dash-dotted) and imbalance (dashed). The bottom friction term collapses with the zero line in the right panel. Units are 10^{-11} m s^{-3} for the QPV flux, 10^{-4} m^2 s^{-2} for the thickness flux.

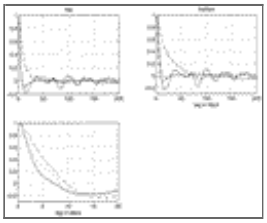

Click on thumbnail for full-sized image.

Fig. 9. Autocorrelation functions (upper panels) of the meridional velocity at five latitudes for EFB. Center $y = 0$ (full), flanks $y = 1/6$ (dash-dotted), and near boundaries $y = 1/3$(dotted and dashed). The crosscorrelation function in the lower panel refers to the center latitude, top autocorrelation (full), bottom autocorrelation (dashed), and cross correlation (dotted).

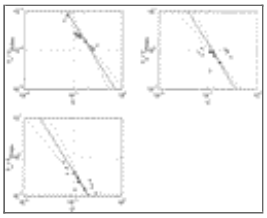

Click on thumbnail for full-sized image.

Fig. 10. Scaling of the $\mathcal{T}_i$ and $\mathcal{T}_\eta$ by the Phillips timescale, plotted vs the mean shear U. Values from the channel center are taken (*FB: "*," *G4: "×," *B5: "+"). Power law dependence U^{-p} is indicated by the straight lines [$p = -2$ (full), $p = -5/2$ and $p = -3/2$ (dotted), centered on experiment EFB].

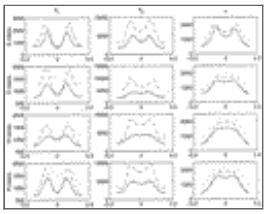

Click on thumbnail for full-sized image.

Fig. 11. Numerically determined eddy diffusivities k_i and κ as function of the scaled latitude y/Y, in units of m^2 s^{-1}. The curves are for *FB cases (full), *G4 cases (dash-dotted), and *B5 cases (dotted), respectively. Values from boundary layers are omitted.

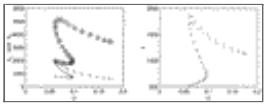

Click on thumbnail for full-sized image.

Fig. 12. Numerically determined eddy diffusivities k_i and κ vs the mean vertical shear U for EFB. Diffusivities are in units of m^2 s^{-1}, units for shear m s^{-1}. Values from boundary layers are omitted. Shown are the values on the y gridpoints, due to the approximate symmetry of the flow the points occur in doublets. Values for the top layer are dotted, for bottom layer plotted as circles.

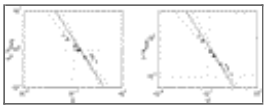

Click on thumbnail for full-sized image.

Fig. 13. Scaling of the diffusivities k_2 and κ by the Green–Stone scaling (21) with Eady timescale, plotted vs the mean shear U. Values from the channel center are compared for all experiments (*FB: "*," *G4: "×," *B5: "+"). Power law dependence U^{-p} is indicated by the straight lines [$p = -2$ (full), $p = -5/2$ and $p = -3/2$ (dotted), centered on experiment EFB].

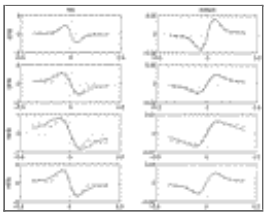

Click on thumbnail for full-sized image.

Fig. 14. The triple moment flux of the QPV flux balance for EFB, DFB, NFB, and HFB, together with the parameterized form (24) and (25). Data from the numerical experiments (full), and advective parameterization (24) (dashed). Units are 10^{-7} m^2 s^{-3}. Values from boundary layers are omitted.

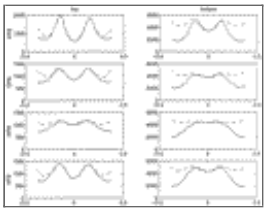

Click on thumbnail for full-sized image.

Fig. 15. Comparison of the rhs and lhs of (27) for the experiments EFB, DFB, NFB, and HFB: k_i (full), and $K_i[1 + \gamma_i(\partial^2\overline{u}_i/\partial y^2)/(\partial\overline{q}_i/\partial y)]$ (dash-dotted). Values from boundary layers are omitted. Units are m^2 s^{-1}.

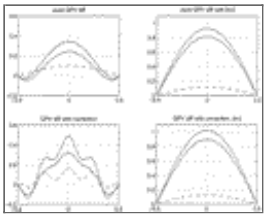

Click on thumbnail for full-sized image.

Fig. 16. Analytical solution of the coarse model (28) for the parameters of EFB (see Table 3). In the upper panels conventional QPV diffusion is used ($\gamma_i = 0$), in in the lower panels the correction term is implemented. We compare a β-plane flow (left panels) with a f-plane flow (right panels). The velocities $\overline{u}_i$ are full, the shear U is dash-dotted. Units are meters per second.

[1] The upper sign of ± and $\overline{+}$ refers to the upper layer and the lower sign to the lower layer.

[2] The first relation in (12) is often used to evaluate *w*. Remember, however, that (11) is based on this equation. Implementing (12) into (11) just regains the triple and production terms. It is also customary but not very meaningful to utilize the ageostrophic momentum balance again to diagnose the ageostrophic fluxes in (13).

[3] The growth rate of the most unstable mode for two-layer Phillips model, expanded at the critical shear $U = \beta\lambda^2_2$, is given by[r1$\beta(U - \beta\lambda$22) times a function of layer depths, which is of order unity.

[4] See Fig. 13 in Ivchenko et al. (1997). Their solution, however, looks very much like the solution of linear QPV diffusion with constant diffusivity shown in the upper left panel of Fig. 16 of this paper.

[5] With unequal layer depths the supercriticality of the Phillips model is $U/(\beta\lambda^2_2)$, which differs by the factor $H_1/(H_1 + H_2)$ from ξ.

[6] We ignore here that K_i does not satisfy the proper boundary condition $K_i(y = \pm Y/2) = 0$.

* Alfred Wegener Institute Contribution Number 1328.

+ Current affiliation: ICBM, Oldenburg, Germany.

Corresponding author address: Dr. Dirk Olbers, Alfred-Wegener-Institute for Polar and Marine Research, Postfach 120161, 27515 Bremerhaven, Germany.

E-mail: dolbers@awi-bremerhaven.de

top